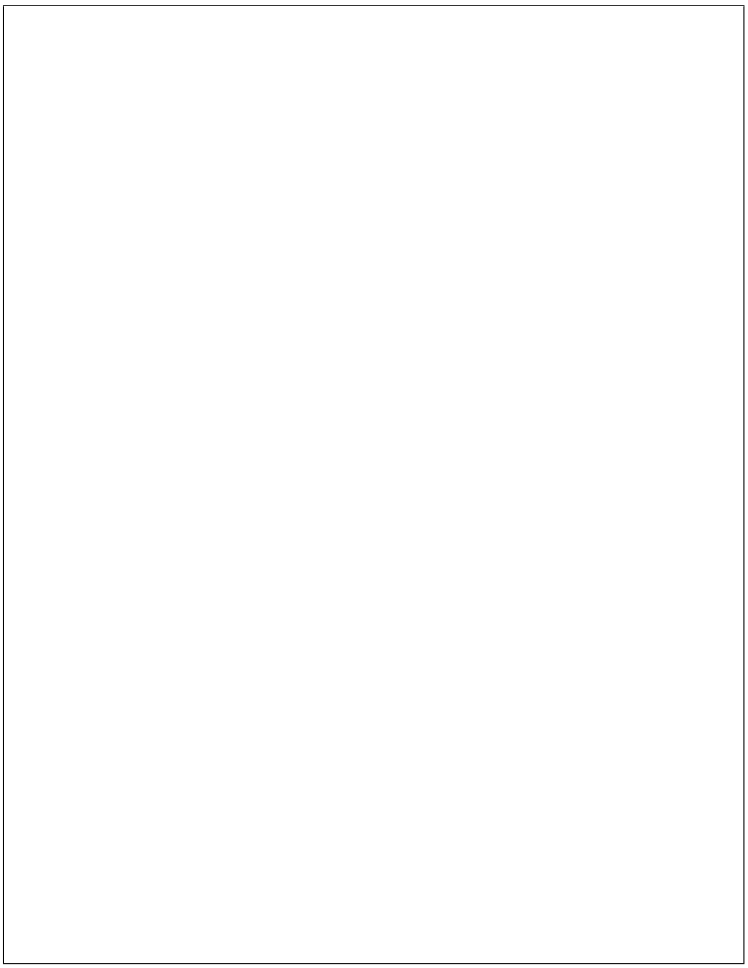

Graphical Models 72 (2010) 61–73

Contents lists available at ScienceDirect

Graphical Models

journal homepage: www.elsevier.com/locate/gmod

Determination of elasticity parameters in lumped element (mass-spring) models of deformable objects

Suriya Natsupakpong *, M. Cenk Çavuşoğlu

Department of Electrical Engineering and Computer Science, Case Western Reserve University, Cleveland, OH 44106, USA

ARTICLE INFO

Article history:
Received 19 March 2010
Received in revised form 4 October 2010
Accepted 7 October 2010
Available online 15 October 2010

Keywords:
Deformable object models
Deformable object simulation
Lumped element models
Mass-spring models
Elasticity parameters
Surgical simulation

ABSTRACT

Lumped element models, also known as, mass-spring-damper models, are widely used to simulate deformable objects because of their simplicity and computational efficiency. However, the parameters of lumped element models are typically determined in an ad hoc fashion through trial-and-error, as these models are not directly based on continuum mechanics of deformable objects. In this paper, an alternative method to determine the elasticity parameters of lumped element models of deformable objects is presented. The elasticity parameters are determined using an optimization that minimizes the matrix norm of the error between the stiffness matrices of the linear lumped element model and the linear finite element model of the same object. The method has been developed for two-dimensions and for three-dimensional volumetric objects with tetrahedral and hexahedral (brick) elements. The method has been validated by comparing deformation results of the lumped element models with the deformation results given by finite element models, under various tension, and compression loading conditions.

1. Introduction

Dynamic simulation of deformable objects in real-time for interactive virtual environments is an active area of research. The application that motivate this study is the development virtual environment-based surgical training simulators, where real-time deformable tissue simulation is one of the enabling technologies. Effective virtual surgical environments require an interactive 3D simulation environment, where the surgeons, using a haptic interface, can manipulate dynamically and geometrically correct models of organs and tissues simulated on a computer.

In this paper, we present a method to determine the mass and spring constants of lumped element (also known as mass-spring) models of deformable objects. The proposed method to determine component parameters is based on approximating the input–output relations of finite element model "elements" with lumped element model "elements." The spring constants are determined through an optimization that minimizes the matrix norm of the error between the stiffness matrices of the lumped element model and the corresponding finite element model of the same object.

1.1. Deformable tissue modeling

The deformable tissue modeling approaches in the literature can be grouped in the following four broad categories: lumped element models (also known as mass-spring-damper models), finite element models (linear and nonlinear), particle based models, and parametric models.

Lumped element models (LEM) are meshes of mass, spring and damper elements (e.g. [1–3]). Lumped element models are the most popular models for real-time surgical simulators, because they are natural extensions of other deformable models used in computer animation. Lumped element models are conceptually simple, and it is possible to construct models which can be simulated at interactive speeds with these type of models. There are many

* Corresponding author.
E-mail addresses: suriya.natsupakpong@case.edu (S. Natsupakpong), cavusoglu@case.edu (M. Cenk Çavuşoğlu).

1524-0703/$ - see front matter © 2010 Elsevier Inc. All rights reserved.
doi:10.1016/j.gmod.2010.10.001

applications used lumped element model, for example, Provot [4] used a mass and spring system to model a deformable cloth. Bourguignon and Cani [5] presented a method to controlling anisotropy of mass-spring system in volumetric deformable models, such as human organs.

Finite element models (FEM) are used as a step to get closer to using models with physically based parameters (e.g. [6–8]). Linear finite element models are computationally attractive as superposition can be used and it is possible to perform extensive off-line calculations to significantly reduce the real-time computational burden. However, linear models are based on the assumption of small deformation, typically less than 1%, which is not valid for much of the soft tissue manipulation during surgery. These models cannot handle rigid motions either [9]. Linear models lose their computational advantage under topology changes, e.g., as a result of cutting, as the off-line calculations cannot be used. To address this last problem, Delingette et al. [10] proposed to use lumped element models locally where there is topological change (such as cutting) and use a linear finite element model for the rest. Nonlinear finite element models are highly accurate models, which take into account nonlinear constitutive behavior of the materials as well as large deformation effects. They are generally regarded as the gold standard for high accuracy computation. However, these models are computationally very intensive and therefore not suitable for real-time simulation in their basic form [11,12,9]. Recently, a lot of research effort has been focusing on improving computational performance of these models. For example, Wu et al. proposed to use mass lumping and adaptive mesh refinement [13], and multigrid simulation [14] to achieve higher performance with nonlinear FEM. Müller et al. [15,16] proposed a corotation-based approach for finite element models to improve the artifacts from large deformation. Nesme et al. [17] presented a FEM-based physically plausible modeling method. As well as, Irving et al. [18] presented an invertible finite element algorithm for simulating large deformations.

Particle based models model the deformable object continuum as a collection of loosely coupled finite volume particles, such as simulating a deformable object as a collection of elastic spheres (for example, as proposed by Conti [19]). The interaction of these particles between themselves and with the external forces determine the behavior of the deformable object. These models are not really intended to accurately model real tissue behavior, but to have a plausible looking tissue behavior achieved through minimal computation.

Parametric models include commonly used free form [20] and spline based [21] deformable models where location of some control points determine locally the shape of the deformable object. Another method for parametric modeling of deformable objects is proposed by Metaxas [3] where a very small number of parameters characterize globally the shape of a large geometric model of a deformable body, e.g. using the semi-axis lengths and principal-axes directions to parametrize an ellipsoid. Parametric models are not physically based, and like particle based models, not intended to accurately model real tissue behavior, but to have fast and plausible looking interactive responses.

1.2. Parameter determination in literature

The two most commonly used deformable object models are finite element models and lumped element models. As mentioned earlier, lumped element models are conceptually simple and computationally more efficient compared to finite element models. A common problem with the lumped parameter models used in literature is the selection of component parameters, spring and damper constants, and nodal mass values. There is no general physically based or systematic method in the literature to determine the element types or parameters from physical data or known constitutive behavior. The typical practice in the literature is somewhat *ad hoc*, the element types and connectivities are empirically assumed, usually based on the structure of the geometric model at hand, and the element parameters are either hand tuned to get a reasonable looking behavior or estimated by a parameter optimization method to fit the model response to an experimentally measured response. For example, Joukhadar et al. [22,23] used a predefined mesh topology and then determined the element parameters with a genetic algorithm search technique. Bianchi et al. [24,25] used a genetic algorithm based method to determine the mesh topology and stiffness of mass-spring models by using finite element models as reference. Deussen et al. [26] used a search method based on simulated annealing algorithm to determine optimum mass-spring parameters in two-dimensions.

There are several studies in the literature which determine lumped element model parameters by using continuum mechanics, elasticity and finite element theory. Gelder [27] proposed a formulation to approximate the spring constants in triangular mesh of isotropic, linearly elastic materials, which he also extended to three-dimensions. The experimental results showed that his model can approximate the deformation of an isotropic elastic membrane with limit condition of Poisson's ratio of zero. Maciel et al. [28] proposed techniques to model a soft tissue from real biological tissue properties by using a generalized mass-spring model (molecular model) with four different methods; however, none of these methods worked unconditionally. Baudet et al. [29,30] proposed an approach similar to Gelder but for rectangular elements. They introduced a correction force orthogonal to the elongation force to correct the effects of non-zero Poisson's ratio and compared results with finite element model simulations. In 2000, Cavusoglu [31], co-author, proposed a method to determine elasticity parameters of a lumped element (mass-spring) model by approximating the stiffness matrix of the finite element model with the stiffness matrix of the lumped element model. More recently, Lloyd et al. [32] introduced a method for identification of spring constants of lumped element models from the finite element models in triangular, rectangular, and tetrahedral meshes. Their method produced the better approximative results when the spring constants had been calculated for the specific value of Poisson's ratio with pre-strained springs in two-dimensional element (rectangular meshes), and with volume preserving forces in three-dimensional element (tetrahedral meshes). Wang and Devarajan [33,34] presented mass-spring models for one and two-dimensions

derived from explicit continuum expressions with a preloaded spring model to improve the accuracy. Delingette [35,36] show that under small deformation and when poisson ratio is equal to 1/3, spring-mass models can be compared to St. Venant Kirchoff hyperelastic materials, providing explicit formulae for spring stiffnesses as well as for angular and volumetric springs that are necessary to represent shearing deformations.

Our method uses an approach similar to the methods of [31,32]. However, the method proposed in this study uses an optimization to find the lumped element model parameters that best fit the finite element model response, while the method presented in [32] calculated the lumped element model parameters from equating the stiffness matrices from lumped element and finite element model. Furthermore, in the present study, the method has also been developed for tetrahedral and hexahedral elements, whereas [32] is limited only to tetrahedral elements. The proposed method is developed for two-dimensions with triangular and quadrilateral elements and for three-dimensional volumetric objects with tetrahedral and hexahedral (brick) elements.

The rest of the paper is organized as follows. In Section 2, the formulation of the soft object deformation using FEM and LEM is compared to make some basic observations and the proposed method is presented in detail. In Section 3, the experimental results are presented, followed by concluding remarks in Section 4. In Appendix A, the finite element and lumped element models are summarized in order to formulate the problem and introduce the notations.

2. Determination of parameters

In finite element models, the parameters of the elements are determined from the constitutive properties of the material of the object being simulated. For the lumped element models, there is no intrinsic method to determine the element parameters since the models are not actually motivated from approximating the physical behavior of the object.

As mentioned in the discussion above, one of the main problems of LEM is the lack of a systematic way to determine element parameters. In the literature, the parameters of the LEM models are determined through parameter estimation, to fit the response of the model to an experimentally measured response. If the structure allows, it may be possible to isolate effects of some parameters or do some approximations to isolate these parameters and therefore simplify parameter estimation [37]. Otherwise, this can be a very complex optimization problem depending on the number of parameters used.

Here, we will establish a parallelism between the elements in FEM and LEM, and explore methods for setting up of the LEM mesh and selection of its parameters as a way to approximate FEM. In the discussion below, without loss of generality, we look at the two-dimensional case (plane strain[1]) in the absence of external forces as an illustrative example, in order to simplify the notation and equations.

Consider a planar 4 node C^0 continuous isoparametric element for the FEM, and a 4 mass configuration for the LEM (Fig. 1). The masses of the LEM mesh are located at the same spatial locations as the nodes of the FEM element. This configuration of the LEM masses, with the interconnection springs and dampers, will be used as the building block elements of the LEM mesh. At this point, we are not yet specifying the spring connections between the nodes.

The equations of motion for the FEM and LEM elements, as given in Section A, are

$$M^e\ddot{\hat{\mathbf{x}}}^e + R^e(\hat{\mathbf{x}}^e) = 0,$$

$$\begin{bmatrix} m_1 & & 0 \\ & \ddots & \\ 0 & & m_4 \end{bmatrix} \ddot{\hat{\mathbf{x}}} + K^e(\hat{\mathbf{x}}) = 0, \tag{1}$$

where superscript 'e' is used to denote element quantities. The matrix M^e is dense, but if we use nodal quadrature, it is possible to get a diagonal approximation for the M^e in FEM. This is a commonly used approximation in FEM to improve computational efficiency (e.g [13]). For the LEM, we can choose

$$m_i = m^e_{ii}, \tag{2}$$

therefore getting a physically based value for the nodal mass. Then, if we can approximate $R^e(\hat{\mathbf{x}}^e)$ with $K^e(\hat{\mathbf{x}})$, we can use the LEM for approximating FEM, avoiding the parameter determination problem. If we look at the structure of the function $R^e(\hat{\mathbf{x}}^e)$,

$$R^e(\hat{\mathbf{x}}^e) = \begin{bmatrix} R^e_1(\mathbf{x}^e_1, \mathbf{x}^e_2, \mathbf{x}^e_3, \mathbf{x}^e_4) \\ R^e_2(\mathbf{x}^e_1, \mathbf{x}^e_2, \mathbf{x}^e_3, \mathbf{x}^e_4) \\ R^e_3(\mathbf{x}^e_1, \mathbf{x}^e_2, \mathbf{x}^e_3, \mathbf{x}^e_4) \\ R^e_4(\mathbf{x}^e_1, \mathbf{x}^e_2, \mathbf{x}^e_3, \mathbf{x}^e_4) \end{bmatrix}, \tag{3}$$

and comparing the FEM equations with the LEM equations,

$$R^e_i(\hat{\mathbf{x}}^e) = \int_{\Omega^e_0} B^{eT}_i S(\hat{\mathbf{x}}^e) dV,$$
$$K^e_i(\hat{\mathbf{x}}) = \sum_{\{i,j\text{connected}\}} \mathbf{f}(\mathbf{x}_i, \mathbf{x}_j), \tag{4}$$

we observe that the nonlinear functions $R^e_i(\hat{\mathbf{x}}^e)$ needs to be approximated by the function $K^e_i(\hat{\mathbf{x}})$, which is the negative

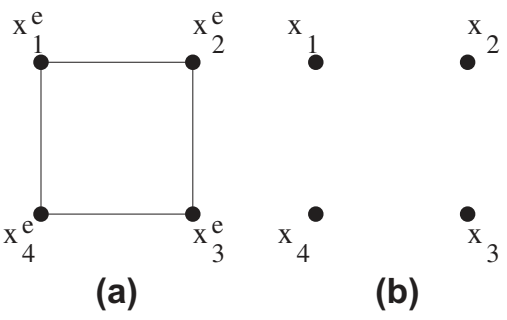

Fig. 1. Four node FEM (a) and LEM (b) elements.

[1] Plane strain analysis is used to solve deformation in infinitely long structures which are uniform in the third dimension.

of the sum of the spring forces on node i. Performing an optimization over the nonlinear functions $R_i^e(\hat{\mathbf{x}}^e)$ and $K_i^e(\hat{\mathbf{x}})$ would be computationally complex. Instead, we will linearize the two models, and perform an optimization to identify the LEM parameters that will most closely match the linearization. This will actually have the effect of matching the tangent behavior of the two original nonlinear models. Also, the linear case will enable us to make some basic observation, which will give us important insights.

For the LEM element, we need to linearize expression for the spring forces by using Taylor series expansion. The result is

$$\begin{bmatrix}\Delta\mathbf{f}_i\\ \Delta\mathbf{f}_j\end{bmatrix} = \begin{bmatrix}\frac{\partial\mathbf{f}(\mathbf{x}_i,\mathbf{x}_j)}{\partial\mathbf{x}_i} & \frac{\partial\mathbf{f}(\mathbf{x}_i,\mathbf{x}_j)}{\partial\mathbf{x}_j}\end{bmatrix}\begin{bmatrix}\mathbf{u}_i\\ \mathbf{u}_j\end{bmatrix}, \tag{5}$$

where $\mathbf{u} = \mathbf{x} - \mathbf{x}(0)$ is the displacement,

$$\frac{\partial\mathbf{f}(\mathbf{x}_i,\mathbf{x}_j)}{\partial\mathbf{x}_i} = -\frac{\partial\mathbf{f}(\mathbf{x}_i,\mathbf{x}_j)}{\partial\mathbf{x}_j} = \begin{bmatrix}A_1^{\mathbf{u}_i,\mathbf{u}_j} & B_{1,2}^{\mathbf{u}_i,\mathbf{u}_j}\\ B_{2,1}^{\mathbf{u}_i,\mathbf{u}_j} & A_2^{\mathbf{u}_i,\mathbf{u}_j}\end{bmatrix}, \tag{6}$$

$$A_p^{\mathbf{u}_i,\mathbf{u}_j} = k^{i,j}\left(1 - \frac{L_0}{\|\mathbf{x}_j-\mathbf{x}_i\|}\frac{\|\mathbf{x}_j-\mathbf{x}_i\|^2 - (\mathbf{x}_{jp}-\mathbf{x}_{ip})^2}{\|\mathbf{x}_j-\mathbf{x}_i\|^2}\right), \tag{7}$$

$$B_{p,q}^{\mathbf{u}_i,\mathbf{u}_j} = k^{i,j}\left(\frac{L_0}{\|\mathbf{x}_j-\mathbf{x}_i\|}\frac{(\mathbf{x}_{jp}-\mathbf{x}_{ip})(\mathbf{x}_{jq}-\mathbf{x}_{iq})}{\|\mathbf{x}_j-\mathbf{x}_i\|^2}\right). \tag{8}$$

Define

$$K_{i,j} = -\begin{bmatrix}A_1^{\mathbf{u}_i,\mathbf{u}_j} & B_{1,2}^{\mathbf{u}_i,\mathbf{u}_j}\\ B_{2,1}^{\mathbf{u}_i,\mathbf{u}_j} & A_2^{\mathbf{u}_i,\mathbf{u}_j}\end{bmatrix} \tag{9}$$

to simplify the notation. Note that $K_{i,j} = K_{j,i}$. Then, the linearized equations for LEM is

$$K^e(\hat{\mathbf{x}}) \approx K^e\hat{\mathbf{u}}, \tag{10}$$

and the K matrix has entries for each of the springs. For example, if we consider the LEM element of Fig. 2 we get

$$K^e = \begin{bmatrix}K_{1,1} & K_{1,2} & K_{1,3} & K_{1,4}\\ K_{2,1} & K_{2,2} & K_{2,3} & K_{2,4}\\ K_{3,1} & K_{3,2} & K_{3,3} & K_{3,4}\\ K_{4,1} & K_{4,2} & K_{4,3} & K_{4,4}\end{bmatrix}, \tag{11}$$

where $K_{i,i} = -\sum_{j=1,\ j\neq i}^{4} K_{i,j}$.

When the FEM element equations are linearized, we get

$$R^e(\hat{\mathbf{x}}^e) \approx R^e\hat{\mathbf{u}}, \tag{12}$$

$$R^e = \int_{\Omega_0^e} B^{eT}DB^e\,dV, \tag{13}$$

where D is the matrix which transforms strain vector to stress vector ($\sigma = D\varepsilon$). For brevity, we are using the same symbol for the nonlinear function and matrix for the linear case, since they are distinguishable from the context.

At this point, to simplify the calculations, we will further assume that the element in the reference configuration is the same as the master element $\widehat{\Omega}$ (Fig. 3) and the deformable object is a homogeneous linear isotropic material. Then,

$$R^e = \int_{\Omega_0^e} B^{eT}DB^e\,dx\,dy = \int_{\widehat{\Omega}} B^{eT}DB^e|J|d\xi\,d\eta = \int_{-1}^{1}\int_{-1}^{1} B^{eT}DB^e|J|d\xi\,d\eta, \tag{14}$$

$$R_{i,j}^e = \int_{-1}^{1}\int_{-1}^{1} B_i^{eT}DB_j^e|J|d\xi\,d\eta, \tag{15}$$

where J is the Jacobian operator relating the natural coordinate derivatives to the local coordinate derivatives. For an isoparametric element, the shape functions in the natural coordinate are

$$\begin{aligned}N_1^e &= \frac{(1-\xi)(1+\eta)}{4},\\ N_2^e &= \frac{(1+\xi)(1+\eta)}{4},\\ N_3^e &= \frac{(1+\xi)(1-\eta)}{4},\\ N_4^e &= \frac{(1-\xi)(1-\eta)}{4},\end{aligned} \tag{16}$$

and for an isotropic plane strain

$$D = \begin{bmatrix}\lambda+2\mu & \lambda & 0\\ \lambda & \lambda+2\mu & 0\\ 0 & 0 & \mu\end{bmatrix}, \tag{17}$$

$$B_I^e = \begin{bmatrix}N_{I,1}^e & 0\\ 0 & N_{I,2}^e\\ N_{I,2}^e & N_{I,1}^e\end{bmatrix}, \tag{18}$$

where λ and μ are the Lame's constants of the material. If we evaluate (15), we get

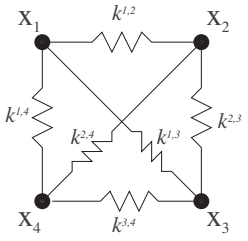

Fig. 2. A fully connected 4 node LEM element.

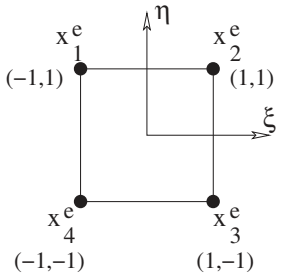

Fig. 3. Four node master FEM element.

$$R^e = \begin{bmatrix}
\frac{\lambda}{3}+\mu & \frac{-\lambda-\mu}{4} & \frac{-\lambda}{3}-\frac{\mu}{2} & \frac{-\lambda}{4}+\frac{\mu}{4} & \frac{-\lambda}{6}-\frac{\mu}{2} & \frac{\lambda}{4}+\frac{\mu}{4} & \frac{\lambda}{6} & \frac{\lambda-\mu}{4} \\
\frac{-\lambda-\mu}{4} & \frac{\lambda}{3}+\mu & \frac{\lambda}{4}-\frac{\mu}{4} & \frac{\lambda}{6} & \frac{\lambda}{4}+\frac{\mu}{4} & \frac{-\lambda}{6}-\frac{\mu}{2} & \frac{-\lambda+\mu}{4} & \frac{-\lambda}{3}-\frac{\mu}{2} \\
\frac{-\lambda}{3}-\frac{\mu}{2} & \frac{\lambda}{4}-\frac{\mu}{4} & \frac{\lambda}{3}+\mu & \frac{\lambda}{4}+\frac{\mu}{4} & \frac{\lambda}{6} & \frac{-\lambda}{4}+\frac{\mu}{4} & \frac{-\lambda}{6}-\frac{\mu}{2} & \frac{-\lambda}{4}-\frac{\mu}{4} \\
\frac{-\lambda}{4}+\frac{\mu}{4} & \frac{\lambda}{6} & \frac{\lambda}{4}+\frac{\mu}{4} & \frac{\lambda}{3}+\mu & \frac{\lambda}{4}-\frac{\mu}{4} & \frac{-\lambda}{3}-\frac{\mu}{2} & \frac{-\lambda}{4}-\frac{\mu}{4} & \frac{-\lambda}{6}-\frac{\mu}{2} \\
\frac{-\lambda}{6}-\frac{\mu}{2} & \frac{\lambda}{4}+\frac{\mu}{4} & \frac{\lambda}{6} & \frac{\lambda}{4}-\frac{\mu}{4} & \frac{\lambda}{3}+\mu & \frac{-\lambda}{4}-\frac{\mu}{4} & \frac{-\lambda}{3}-\frac{\mu}{2} & \frac{-\lambda}{4}+\frac{\mu}{4} \\
\frac{\lambda}{4}+\frac{\mu}{4} & \frac{-\lambda}{6}-\frac{\mu}{2} & \frac{-\lambda}{4}+\frac{\mu}{4} & \frac{-\lambda}{3}-\frac{\mu}{2} & \frac{-\lambda}{4}-\frac{\mu}{4} & \frac{\lambda}{3}+\mu & \frac{\lambda}{4}-\frac{\mu}{4} & \frac{\lambda}{6} \\
\frac{\lambda}{6} & \frac{-\lambda+\mu}{4} & \frac{-\lambda}{6}-\frac{\mu}{2} & \frac{-\lambda}{4}-\frac{\mu}{4} & \frac{-\lambda}{3}-\frac{\mu}{2} & \frac{\lambda}{4}-\frac{\mu}{4} & \frac{\lambda}{3}+\mu & \frac{\lambda+\mu}{4} \\
\frac{\lambda-\mu}{4} & \frac{-\lambda}{3}-\frac{\mu}{2} & \frac{-\lambda}{4}-\frac{\mu}{4} & \frac{-\lambda}{6}-\frac{\mu}{2} & \frac{-\lambda}{4}+\frac{\mu}{4} & \frac{\lambda}{6} & \frac{\lambda+\mu}{4} & \frac{\lambda}{3}+\mu
\end{bmatrix}. \tag{19}$$

We can make one observation here, on how to determine the required connectivity of the LEM elements. The matrix R^e does not have a zero block. This is because the degrees of freedom in this FEM element are all coupled. Therefore, for the LEM element to be able to have a behavior similar to the FEM element, it needs to be fully connected, as shown in Fig. 2.

Since the material is assumed to be isotropic, the LEM element has to be symmetric and K^e has only two independent parameters, k^{edge} and k^{diag}, as the following

$$k^{edge} = k^{1,2} = k^{2,3} = k^{3,4} = k^{4,1}, \tag{20}$$

$$k^{diag} = k^{1,3} = k^{2,4}. \tag{21}$$

If we evaluate (9), we get

$$K^e = \begin{bmatrix}
k^{aa} & -\frac{k^{dd}}{2} & -k^{ee} & 0 & -\frac{k^{dd}}{2} & \frac{k^{dd}}{2} & 0 & 0 \\
-\frac{k^{dd}}{2} & k^{aa} & 0 & 0 & \frac{k^{dd}}{2} & -\frac{k^{dd}}{2} & 0 & -k^{ee} \\
-k^{ee} & 0 & k^{aa} & \frac{k^{dd}}{2} & 0 & 0 & -\frac{k^{dd}}{2} & -\frac{k^{dd}}{2} \\
0 & 0 & \frac{k^{dd}}{2} & k^{aa} & 0 & -k^{ee} & -\frac{k^{dd}}{2} & -\frac{k^{dd}}{2} \\
-\frac{k^{dd}}{2} & \frac{k^{dd}}{2} & 0 & 0 & k^{aa} & -\frac{k^{dd}}{2} & -k^{ee} & 0 \\
\frac{k^{dd}}{2} & -\frac{k^{dd}}{2} & 0 & -k^{ee} & -\frac{k^{dd}}{2} & k^{aa} & 0 & 0 \\
0 & 0 & -\frac{k^{dd}}{2} & -\frac{k^{dd}}{2} & -k^{ee} & 0 & k^{aa} & \frac{k^{dd}}{2} \\
0 & -k^{ee} & -\frac{k^{dd}}{2} & -\frac{k^{dd}}{2} & 0 & 0 & \frac{k^{dd}}{2} & k^{aa}
\end{bmatrix}, \tag{22}$$

where $k^{ee} = k^{edge}$, $k^{dd} = k^{diag}$, and $k^{aa} = \frac{k^{diag}}{2} + k^{edge}$. R^e for the FEM element also has two independent parameters, namely, Lame's constants, λ and μ. Then, at first we may think that it should be possible to construct the LEM element which has the same input–output behavior as the FEM element. However, it is not too difficult to see that this is not true, if we look at the individual terms of the matrices K^e and R^e. Each subblock $R^e_{i,j}$ depends on both of the parameters (λ, μ), but this is not the case for $K^e_{i,j}$, which depends only on single parameter ($k^{i,j}$). Therefore, in block by block sense, the LEM element cannot represent the Poisson's ratio and bulk modulus simultaneously.

The difference between the behavior of the FEM and LEM elements comes from the fact that the interaction between the nodes are restricted to be some form of spring-like behavior in LEM, whereas there is freedom in FEM. This restricts the physical material behavior that LEM models can represent.

It is also possible to consider adding angular springs within the LEM element. This would enrich the behavior of the LEM element. However, addition of angular springs would decrease the computational attractiveness of the LEM because of the increased computational complexity. We will leave this for future work.

To approximate FEM element behavior with an LEM element, at least for the linear case, we need to perform the following optimization

$$(k^{edge}, k^{diag}) = \arg \inf_{k^{edge}, k^{diag}} \|R^e(\lambda,\mu) - K^e(k^{edge}, k^{diag})\| \tag{23}$$

in some norm. There are two different norms used in this paper, which are the Frobenius norm and induced 2-norm. Specifically, for a given displacement vector, u, $f_{FEM} = R^e u$ gives the nodal forces for the FEM model, and $f_{LEM} = K^e u$ gives the nodal forces of the LEM model of the element. The difference of the two force vectors, which is the output force error between the two models, can be calculated by

$$f_{FEM} - f_{LEM} = R^e u - K^e u = (R^e - K^e)u. \tag{24}$$

Then, the induced 2-norm of the matrix $(R^e - K^e)$, i.e.

$$\|R^e - K^e\|_2 = \sup_u \frac{\|(R^e - K^e)u\|_2}{\|u\|_2}, \tag{25}$$

give the largest force error between the two models, in the sense of the Euclidean norm of the force vectors, that can be produced by applying unit magnitude input displacements, u. Thereforce, minimizing the induced 2-norm of the $(R^e - K^e)$ matrix would yield the set of LEM model parameters that would minimize error between the input–output relationships of the LEM and FEM models. The Frobenius norm of a matrix is the square root of the sum of squares of the elements of a matrix. Minimizing the Frobenius norm of the matrix $(R^e - K^e)$ tries to match the responses of the LEM and FEM models by trying to minimize the term by term difference between individual entries of the two stiffness matrices.

For this particular example, if we use the Frobenius norm, the blocks will be decoupled, and we can get a simple closed form solution for the k^{edge} and k^{diag} values that minimize the error:

$$R^e_{1,2} = \begin{bmatrix} -\frac{\lambda}{3}-\frac{\mu}{2} & -\frac{\lambda}{4}+\frac{\mu}{4} \\ \frac{\lambda}{4}-\frac{\mu}{4} & \frac{\lambda}{6} \end{bmatrix},$$

$$K^e_{1,2} = \begin{bmatrix} -k^{edge} & 0 \\ 0 & 0 \end{bmatrix} \tag{26}$$

gives

$$k^{edge} = \frac{\lambda}{3} + \frac{\mu}{2}, \tag{27}$$

and

$$R^e_{1,3} = \begin{bmatrix} -\frac{\lambda}{6} - \frac{\mu}{2} & \frac{\lambda}{4} + \frac{\mu}{4} \\ \frac{\lambda}{4} + \frac{\mu}{4} & -\frac{\lambda}{6} - \frac{\mu}{2} \end{bmatrix},$$

$$K^e_{1,3} = \frac{1}{2}\begin{bmatrix} -k^{diag} & k^{diag} \\ k^{diag} & -k^{diag} \end{bmatrix} \tag{28}$$

gives

$$k^{diag} = \left(\frac{\lambda}{6} + \frac{\mu}{2}\right) + \left(\frac{\lambda}{4} + \frac{\mu}{4}\right) = \frac{5\lambda}{12} + \frac{3\mu}{4} \tag{29}$$

for the element configurations we assumed.

At this point, it is important to observe that, even though it is possible to find a unique (k^{edge}, k^{diag}) pair for every (λ, μ), it is not possible to make the error equal to zero. This is because of the fact that the stiffness matrices of FEM "elements" and LEM "elements" are structurally different. Therefore, it is not possible to select LEM parameter to exactly match the FEM behavior even though they may have same number of parameters.

If we use the 2-norm or consider different element geometries, the unknown parameters will not be decoupled, and we cannot get a closed form solution; therefore, optimization techniques need to be used to find the best solution. This optimization to determine LEM parameters need to be performed for every different element configuration, since the linearization depends on the geometry of the elements.

We can summarize the proposed method as follows:

1. We will construct the LEM of the deformable object as composed of "elements" or building blocks that are fully connected, rather than having an arbitrarily connected mass-spring mesh. These building block LEM "elements" will be used to approximate the stiffness characteristic of FEM "elements" of same size and geometry.
2. For each of the LEM "elements":
   (a) A linearized LEM "element" stiffness matrix K^e is calculated using (5)–(10). This stiffness matrix is parameterized by the (unknown) spring constants of the LEM, and gives the tangent behavior of the LEM.
   (b) A FEM element with same geometry as the LEM "element" is constructed. The stiffness matrix R^e for the FEM element is calculated with (A.4), using a linear elastic model (e.g. (A.10)). This FEM stiffness matrix is parameterized by the (known) constitutive parameters of the material, and gives the tangent behavior of the FEM.
   (c) An optimization is performed to identify the LEM element parameters that minimize the error $\|R^e - K^e\|$, similar to (23), using a suitable matrix norm (2-norm or F-norm).
   (d) The nodal mass values of the elements are calculated using (2), where m^e_{ii} are given by (A.4).
3. The LEM is "assembled" by adding the nodal mass values and spring constants for overlapping lumped masses and springs from neighboring "elements".

As these optimizations to identify LEM component parameters are conducted off-line when the object model is constructed, it will not impact the on-line computational efficiency of the LEM. This optimization can also be performed at the whole object level instead of per element. However, this would not be practical as its computation cost will be prohibitively large and it will be prone to local minima problems. Finally, the optimization in step 2(c) can also be performed using the nonlinear forms of $R^e(\hat{\mathbf{x}}^e)$ and $K^e(\hat{\mathbf{x}}^e)$ by evaluating these at a collection of p values, $\hat{\mathbf{x}}^e_i = \hat{\mathbf{x}}_i, i = 1, \ldots, p$, and minimizing a cost function $\sum_{i=1}^{p} \|R^e(\hat{\mathbf{x}}^e_i) - K^e(\hat{\mathbf{x}})\|^2$, defined with a suitable vector norm. However this optimization would also be computationally intensive, and therefore has not been pursued in this paper.

3. Simulation results

In this section, we present simulation results that validate and demonstrate our proposed method. The simulation experiments are implemented by using Mathematica, MATLAB, and C++ with GiPSi framework [38] environments. In our simulation, the simulated objects have the Young's modulus of 10 kPa and the Poisson's ratio of 0.3, unless otherwise stated. In two-dimensional examples, a plane stress case is used. Four different configurations of LEM "element" meshes are considered. In the planar examples, triangular and quadrilateral meshes are used and for three-dimensional volumetric object examples, tetrahedral and hexahedral meshes are used. In order to provide quantitative results, the percentage of root mean square error, $\%e_{rms}$, and the percentage of maximum error, $\%e_{max}$, of Euclidean distance between FEM and LEM nodes are calculated by $\%e_{rms} = \frac{e_{rms}}{o_{max}} * 100$ and $\%e_{max} = \frac{e_{max}}{o_{max}} * 100$, where $e_{rms} = \sqrt{\frac{1}{n}\sum_{i=1}^{n}(x_i^{FEM} - x_i^{LEM})^2}$, $e_{max} = \max|x_i^{FEM} - x_i^{LEM}|$, o_{max} is the maximum Euclidean distance between the undeformed configuration and the deformed configuration of FEM, n is the number of nodes in the models, and x_i^{FEM} and x_i^{LEM} denote the positions of corresponding nodes of the FEM and LEM. In the figures showing simulation results, the color and type of line identifies the object configuration. The original configuration of object is shown with dotted gray lines, the deformed configuration of the FEM is shown with dashed blue lines and the deformed configuration of the LEM is shown with solid red lines. Simulation results which compare the deformation of various two and three-dimensional test objects are reported in Section 3.1. The use of two different matrix norms during the optimization in step 2(c) of the algorithm are also compared in this section. The norms used in this paper are the Frobenius norm and the induced 2-norm. The elastic parameters are calculated symbolically in the Frobenius norm case using Mathematica and numerically in the induced 2-norm case using MATLAB. In Section 3.2, specially designed specimen are used to determine the mechanical properties of object using the proposed method. In Section 3.3, the relationship between the Young's modulus and Poisson's ratio is explored. In Section 3.4, simulation results which compare our method to other similar methods in the literature by using tension, shearing,

and torsion tests are presented. Finally, our method is implemented in real world application to determine the elasticity parameters of lumped element model of third ventricle floor in Section 3.5.

3.1. Test objects

We demonstrate our proposed method with variety of test objects. In the two-dimensional case, we use the object shown in Fig. 4, which represents an arbitrarily shaped soft tissue approximately 2×6 cm^2 in size. In the three-dimensional case, three objects are used. The first object is a cylindrical object with a radius of 1 cm and a height of 2 cm shown in Fig. 5a and b. This object is discretized with tetrahedral (Fig. 5a) and hexahedral (Fig. 5b) elements. The second object is a cylinder with the same dimension as the first object but with an empty spherical hole of radius 0.6 cm inside (Fig. 5c), which is discretized with tetrahedral elements. The third object is a cube with dimensions of $2 \times 2 \times 2$ cm^3 (Fig. 6), which is discretized with tetrahedral (Fig. 6a) and hexahedral (Fig. 6b) elements. In each object, the boundary is kept fixed on one side and the tension forces are applied in opposite side to make the object deformed at least 10% of original configuration. The simulation results are shown in Figs. 4–6 and quantitative results are summarized in Table 1. When we compare the effect of the matrix norm used in the optimization, we observe that the 2-norm has yielded better results in triangular and hexahedral elements, whereas the F-norm has yielded better results in quadrilateral and tetrahedral elements.

In order to illustrate the time complexity of our proposed parameter estimation method, the computation time for each element type and matrix norm is recorded. The computation time is calculated by averaging the time used in finding the solution for 100 randomly constructed elements. The results are shown in Table 2. The computation time when F-norm used is significantly less than the computation time when 2-norm is used. Because the computation for determination by using F-norm can be solved with algebra solver (as illustrated in Section 2), whereas the computation for determination by using 2-norm is performed numerically to find the best solution. The number of spring constants that have to be determined also effects the computational time.

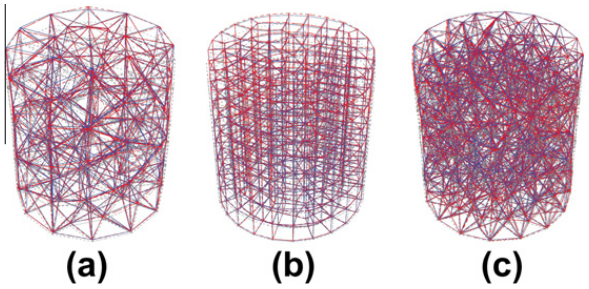

Fig. 5. Three-dimensional test object results (a) cylindrical object with tetrahedral elements calculated using F-norm; (b) cylindrical object with hexahedral elements calculated using 2-norm; and (c) cylindrical object with a hole with tetrahedral elements calculated using F-norm.

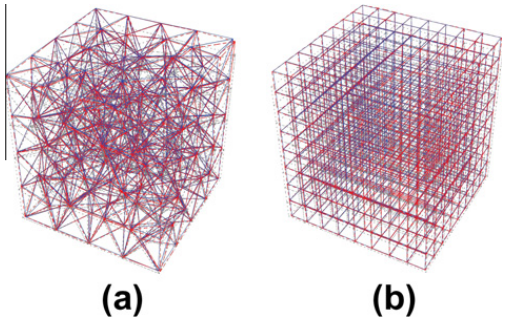

Fig. 6. Three-dimensional test objects (a) cube object with tetrahedral elements calculated using F-norm; and (b) cube object with hexahedral elements calculated using 2-norm.

Finally, a large deformation stretch test was performed to evaluate if the trends illustrated by the earlier experimental results hold for larger object deformations. Specifically, the three-dimensional cube objects with tetrahedral and hexahedral meshes were subjected to 30% stretch deformations. The results (Table 3) show indicate that the trends observed in the earlier results also hold for larger deformations.

3.2. Mechanical tests on specimens

It is also valuable to measure the resulting Young's modulus and Poisson's ratio of the constructed simulation models of objects to evaluate how well they approximate the original values used. In order to accurately measure these parameters, we have conducted mechanical tests

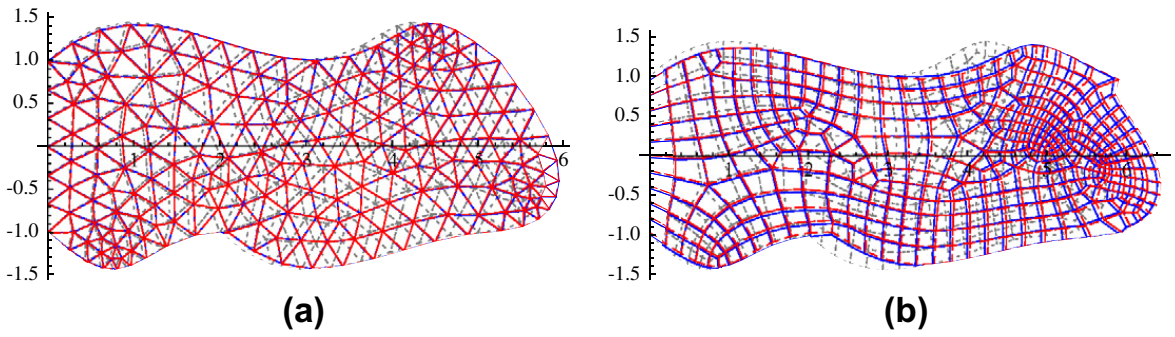

Fig. 4. Two-dimensional test object results (a) mesh with triangular elements calculated using 2-norm; and (b) mesh with quadrilateral elements calculated using with F-norm.

Table 1
Summary of simulation results of test objects.

Test object	Element	Norm	$\%e_{rms}$	$\%e_{max}$	#node	#element
Tissue	tri	2-norm	2.26	4.99	210	366
		F-norm	3.46	6.42		
	qua	2-norm	5.55	9.65	445	405
		F-norm	5.14	8.44		
Cylinder	tet	2-norm	22.89	43.73	124	381
		F-norm	11.00	24.29		
	hex	2-norm	5.63	18.49	675	496
		F-norm	6.15	18.00		
Cylinder with hole	tet	2-norm	20.53	38.96	404	1559
		F-norm	5.91	13.77		
Cube	tet	2-norm	22.52	53.51	170	592
		F-norm	8.28	25.29		
	hex	2-norm	2.91	6.92	729	512
		F-norm	14.98	25.19		

Table 2
Time complexity of each element type with F-norm and 2-norm.

		Time used/element(s)	
Element	#spring constant	F-norm	2-norm
Triangular	3	0.08	1.73
Quadrilateral	6	0.32	2.26
Tetrahedral	6	0.32	2.33
Hexahedral	28	3.04	29.01

Table 3
Large deformation results of cube objects.

Test object	Element	Norm	$\%e_{rms}$	$\%e_{max}$
Cube	Tet	2-norm	22.30	53.35
		F-norm	8.28	25.29
	Hex	2-norm	2.95	14.36
		F-norm	14.98	25.19

on specially designed specimens, following the experimental material characteristic literature. Specifically, the specimen shape chosen is an optimal shape of thin tensile test specimen from [39]. The specimen shape is shown in Fig. 7 with $B = 1$ cm. The thickness of the three-dimensional specimen is 1 cm. The boundary on the left side is kept fixed and the tension force for loading is applied on the right side. The experiment procedure is as follows: First, Young's modulus of 10 kPa and Poisson's ratio of 0.3 are selected. Then, the spring constants of the specimens are determined using the proposed method. The boundary conditions and the loading force are applied to the lumped element model and the displacements of the straight-sided section L_s are collected. These values are then used to calculate the corresponding Young's modulus and Poisson's ratio of specimen. The experimental results shown in Table 4. The results show that the proposed method can represent the Young's modulus close to the desired value in meshes with triangular (2D) and hexahedral (3D) elements with both F-norm and 2-norm and in meshes with quadrilateral and tetrahedral elements with F-norm. The quadrilateral and tetrahedral elements with 2-norm result in error in the Young's modulus more than 10%.

Table 4
Tension tests on specimen.

Element	Norm	E_{out}	v_{out}	#node	#element
Triangular	2-norm	10300.70	0.25	125	192
	F-norm	9461.44	0.26		
Quadrilateral	2-norm	11169.70	0.45	329	266
	F-norm	9839.55	0.43		
Tetrahedral	2-norm	12165.80	0.09	538	1500
	F-norm	9697.49	0.09		
Hexahedral	2-norm	9804.64	0.29	1396	843
	F-norm	10228.00	0.29		

3.3. Control of young's modulus and poisson's ratio in lumped element models

In order the explore the relationship between the Young's modulus and Poisson's ratio of lumped element models and how independently they can be controlled, we conduct another set of tests. Specifically, we use a lumped element model with only one quadrilateral element (with size of 2×2 cm^2) and vary the desired elastic properties ($E_{in} = 1$ Pa to 10 kPa, $v_{in} = 0$–0.5). Then, the elastic properties (E_{out}, v_{out}) of the resulting model is compared with the desired values. The results, show in Fig. 9, reveal that, although it is possible to accurately control the Young's modulus value of the model, it is not possible to

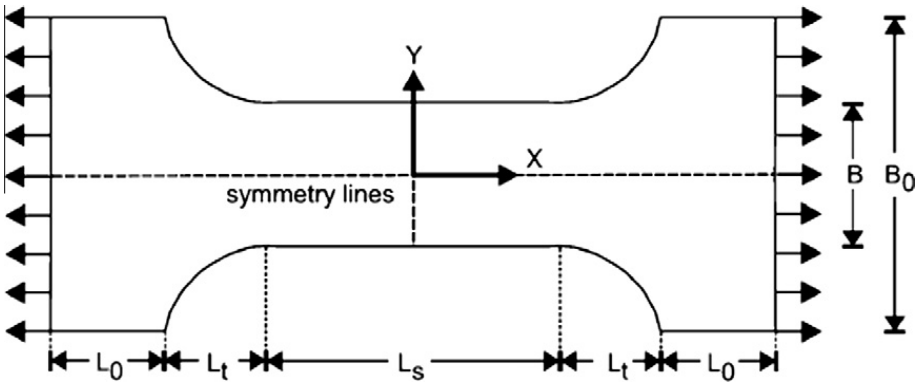

Fig. 7. Specimen shape [39] with $L_s = 2B$, $L_t = 4B$, $L_0 = B_0$, and $B_0 = 3B$.

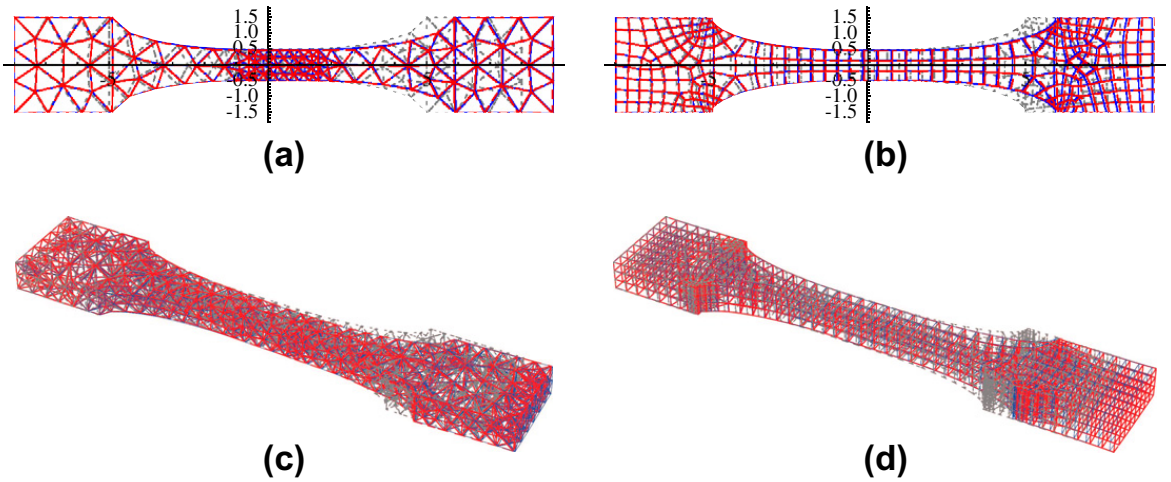

Fig. 8. Tension test on specimens (a) triangular element; (b) quadrilateral element; (c) tetrahedral element; and (d) hexahedral element.

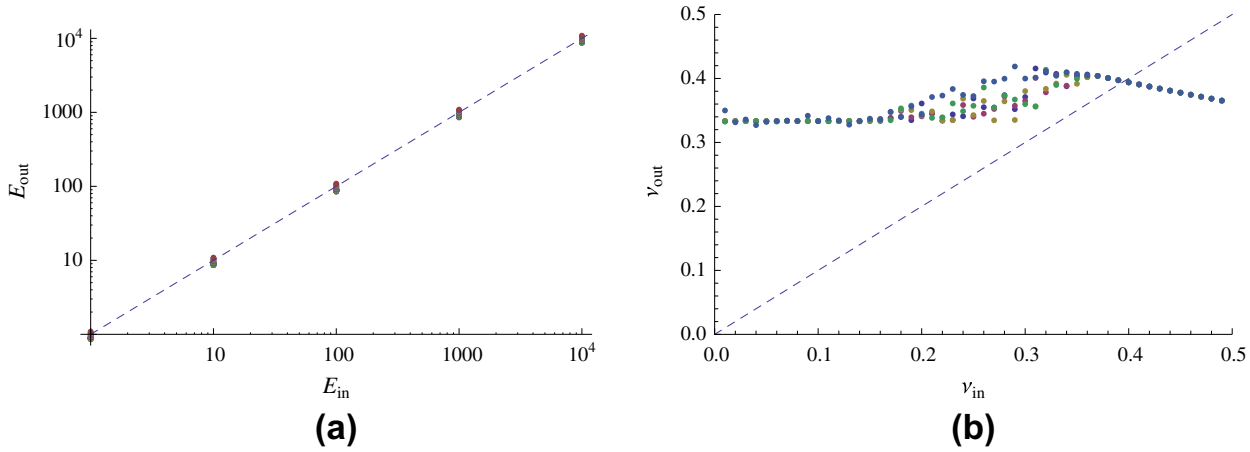

Fig. 9. Young's modulus (a) and Poisson's ratio (b) of lumped element model with quadrilateral element.

independently control the Poisson's ratio. Such a behavior was also observed by other researchers [29,30,32].

3.4. Comparison with other methods

As discussed in Section 1, there are several other studies in the literature that propose methods to determine elasticity parameters in lumped element models. In the two-dimensional case, we compare our proposed method with the methods proposed by Gelder [27] and Lloyd et al. [32] for meshes with triangular elements (test object shows in Fig. 8a), and the methods proposed by Baudet et al. [29] and Lloyd et al. [32] for the meshes with rectangular elements (test object shows in Fig. 8b). We also compare our proposed method in three-dimensional case with the method proposed by Lloyd et al. [32] for meshes with tetrahedral elements (test object shows in Fig. 8c), and with the method proposed by Baudet et al. [30] for meshes with hexahedral elements (test object shows in Fig. 6b).[2] The comparison results are shown in Table 5. The proposed method gives the best result except for the case with quadrilateral elements in two dimension, when it gives the second best result, and the case with tetrahedral element in three dimension. For the quadrilateral mesh case, it should be noted that the method proposed by Baudet et al. introduces a correction force which is not from a spring, and hence it is not a pure lumped element model, and it is

[2] In the case for meshes with hexahedral elements, the object in Fig. 6b was used instead of the test specimen in Fig. 8d, since the method by Baudet et al., was only for uniform (i.e. cubic) shaped elements.

Table 5
Comparison with other methods.

Element	Method	E	ν	$\%e_{rms}$	$\%e_{max}$
Tri	Gelder	15010.80	0.27	20.08	34.58
	Lloyd et al.	10855.80	0.29	5.61	10.88
	Our 2-norm	10300.70	0.25	3.02	5.65
Qua	Baudet et al.	10330.50	0.34	1.06	2.07
	Lloyd et al.	13097.10	0.44	4.84	8.20
	Our 2-norm	11169.70	0.45	3.36	5.50
Tet	Lloyd et al.	8671.48	0.03	7.75	14.65
	Our F-norm	9697.49	0.09	9.37	15.72
Hex	Baudet et al.	10712.50	0.12	3.67	6.99
	Our 2-norm	10242.00	0.14	2.88	6.05

Table 6
Shearing tests in comparison with other methods.

Element	Method	Shearing	
		$\%e_{rms}$	$\%e_{max}$
Tri	Gelder	17.25	34.17
	Lloyd et al.	5.04	10.73
	Our 2-Norm	3.68	8.60
Qua	Baudet et al.	3.60	8.28
	Lloyd et al.	3.64	8.85
	Our 2-Norm	3.82	11.28
Tet	Lloyd et al.	5.68	15.16
	Our F-Norm	5.30	14.55
Hex	Baudet et al.	3.86	9.36
	Our 2-Norm	3.96	9.37

applicable only for "cubic" elements. Also, for the tetrahedral mesh case our proposed method resulted in an effective Young's modulus value which is close to the desired value than the method by Lloyd et al., even though the actual $\%e_{rms}$ value are slightly higher.

We have also performed shearing tests in comparison with other methods. In the two-dimensional case, we use a $2 \times 2\,cm^2$ square object with triangular elements (101 nodes, 168 elements) and with quadrilateral elements (121 nodes, 100 elements). In the three-dimensional case, we use a $2 \times 2 \times 2\,cm^3$ cube object with tetrahedral elements (170 nodes, 592 elements) and with hexahedral elements (729 nodes, 512 elements). The results of these test are given in Table 6. Our proposed method in shearing test gives the best result in triangular and tetrahedral elements, and comparable results in hexahedral element.

3.5. Real world application example

The proposed method to determine the elasticity parameters of lumped element model is implemented and used as part of a prototype surgical simulator, namely, an endoscopic neurosurgery training simulator for the third ventriculostomy procedure. The third ventriculostomy procedure is used for endoscopic treatment of hydrocephalus, a life threatening neurological disorder which is caused by a blockage in the ventricles of the brain and causes an enlargement of the ventricles. Endoscopic third ventriculostomy procedure involves making a hole at the third ventricle floor with a catheter and enlarging the hole with balloon inflation. This procedure allows cerebrospinal fluid to flow normally and reduce the pressure in the brain. The simulator has been developed by using GiPSi framework [38] and tested on the Microsoft Windows XP(TM) 32-bit based workstation with Intel Pentium D 2.80 GHz, 1 GB of RAM and a PCI-express NVidia GeForce 8800 Ultra Graphics Card with 768 MB of memory. The geometric models of the anatomy used in the simulator are obtained from a commercial company. The area of interest, the third ventricle floor, is modeled by a high resolution lumped element model by using parameters determined using the proposed method (Fig. 10a). The overall simulation consisted of 22 simulation objects, 13 texture objects and 3 connectors. The ventricle system model (excluding the floor of the third ventricle) was composed of 9145 nodes and 17942 faces with a quasi static spring model, and the ventricle floor model was composed of 558 nodes and 1050 faces with lumped element model of 558 masses and 1607 springs. The implicit Euler numerical integration method with simulation time step of 0.01 second was used for lumped element model in simulation. The simulator operated at about 30 frames per second (Fig. 10b).

4. Discussion and conclusion

In this paper, a systematic method to determine mass and spring constants of lumped element models of deformable objects is presented. The lumped element model parameters are determined using a finite element model as a reference model by minimizing the error the stiffness matrices of the finite element and lumped element models through an optimization. The proposed method is

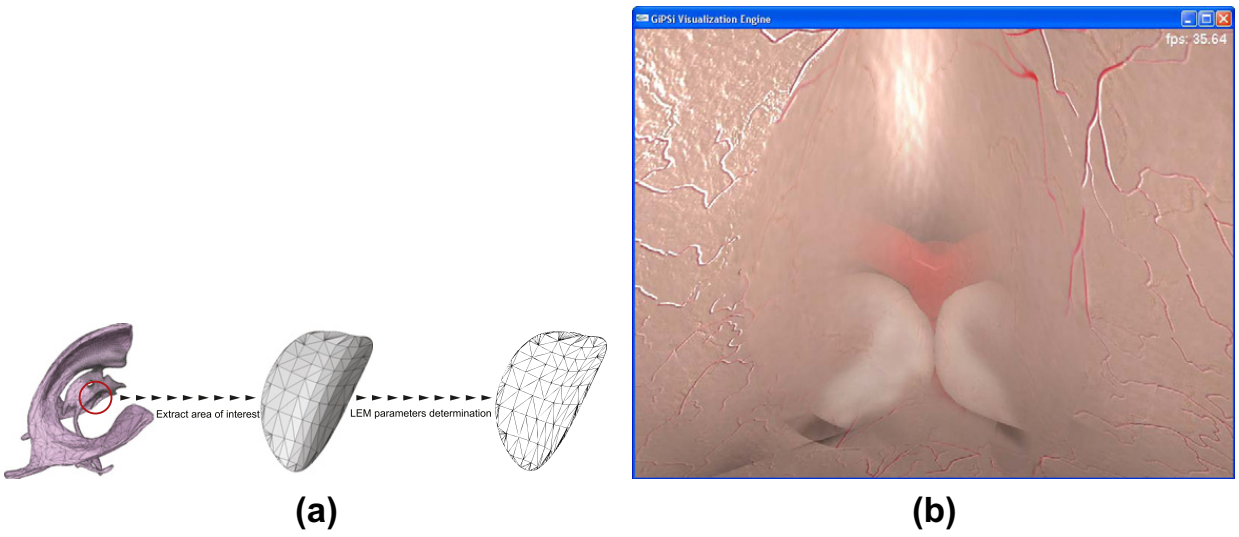

Fig. 10. The proposed method in real world application (a) the third ventricle floor is extracted for creating the lumped element model from geometric model and (b) the third ventricle floor captured from simulation.

demonstrated by several test objects in two and three dimension with triangular, quadrilateral, tetrahedral, and hexahedral elements. Using 2-norm yielded better results in triangular and hexahedral elements, whereas using F-norm yielded better result in quadrilateral and tetrahedral elements. The time complexity by using F-norm is shown to be an order-of-magnitude less than using 2-norm. It is also shown that, with the proposed method, the Young's modulus of the objects are well approximated. However, it is not possible to control the Poisson's ratio of the lumped element model independently as it was also observed by other researchers [29,30,32]. The proposed method is also shown to give results better than or comparable to other existing methods in the literature. The proposed method is also shown to be more flexible than existing methods in the literature as it can be applied to any type of elements in two or three-dimensions, and does not have any underlying assumptions on material parameters.

The proposed method is based on the constructing LEM models using fully connected "elements" which are analogous to elements in FEM models, so that the stiffness behavior of the LEM "elements" are matched to that of FEM elements. Therefore, the presented approach, in its proposed form, is not applicable to interlaced or arbitrarily connected LEM models. The existing approaches in the literature [27,29,30,32] try to derive analytical relationships between LEM model parameters and the underlying material properties. As discussed in Section 2, the LEM models are not structurally capable of representing arbitrary material behaviors. Therefore, such analytical approaches require a priori assumptions that make the analytical derivations possible. For example, for triangular elements, Lloyd et al. assumes that the material has a Poisson ratio of 1/3 and the elements are shaped as equilateral triangles (in Section 3.3 of [32]) in order to be able to match LEM and FEM stiffness matrices. However, such a priori assumptions bias these algorithms to be more accurate under the specific conditions for which the analytical relationships are derived. In contrast, the proposed approach estimates LEM "elements" elasticity parameters numerically by trying to approximate FEM input–output relationships, and therefore, does not rely on such assumptions. It is conjectured that this is the reason that the proposed algorithm produces results better than or comparable to the other existing methods.

Acknowledgments

This research was supported in part by National Science Foundation under Grants CNS-0423253, IIS-0805495, and IIS-0905344, US Department of Commerce under Grant TOP-39-60-04003, Rainbow Foundation, and Cleveland Foundation.

Appendix A. Formulation

The basic FEM and LEM model equations are summarized here in order to clarify the notation and formulations used in the paper, and to aviod any potential errors that may result from different notations used in the literature.

A.1. Finite element models (FEM)

Finite element method is a systematic technique for obtaining the spatial discretization of the partial differential equation describing the continuum behavior of deformable objects. In this section, we will introduce the basic formulation of the finite elements method. Please refer to [40,41] for detailed treatments of the finite elements method. The formulation is based on the total Lagrangian form of the field equations that govern the dynamic behavior of elastic bodies, as given by [42–44].

We will consider the following finite element approximation on each element

$$\mathrm{x}(\mathbf{p},t)=\sum_{I=1}^{\mathrm{NEN}} N_I^e \mathbf{x}_I^e(t), \tag{A.1}$$

where $\mathrm{x}(\mathbf{p},t)$ is the deformation field of the body as a function of the material point coordinates $\mathbf{p}$ and time t, $N_I^e, I=1\cdots\mathrm{NEN}$, is the isoparametric set of approximation functions (shape functions), NEN is the number of node in element, and $\mathbf{x}_I^e, I=1\cdots\mathrm{NEN}$, are the coordinates of the nodes of the element.

At the element level, the FEM model equations are in the form

$$M^e\ddot{\hat{\mathbf{x}}}^e+R^e(\hat{\mathbf{x}}^e)=F^e, \tag{A.2}$$

where

$$\mathrm{x}^e=\begin{bmatrix}\mathbf{x}_1^e\\ \mathbf{x}_2^e\\ \vdots\\ xb_{\mathrm{NEN}}^e\end{bmatrix}, \tag{A.3}$$

and,

$$\begin{aligned}&M^e=\textstyle\int_{\Omega_0^e} N^{eT}\rho_0 N^e dV \quad \text{is the element mass matrix,}\\ &R^e=\textstyle\int_{\Omega_0^e} B^{eT}S(N^e\hat{\mathbf{x}}^e)dV \quad \text{is the stress divergence term,}\\ &F^e=\textstyle\int_{\Omega_0^e} N^{eT}\mathbf{b}_0 dV+\int_{\partial\Omega_0^e\cap S_{2_0}} N^{eT}\bar{\mathbf{s}}dA \quad \text{is the external force vector.}\end{aligned} \tag{A.4}$$

In (A.4),

$$N^e=\begin{bmatrix}N_1^e I & N_2^e I & \cdots & N_{\mathrm{NEN}}^e I\end{bmatrix}, \tag{A.5}$$

$$B^e=\begin{bmatrix}B_1^e & B_2^e & \cdots & B_{\mathrm{NEN}}^e\end{bmatrix}, \tag{A.6}$$

$$B_I^e=\begin{bmatrix}N_{I,1}^e & 0 & 0\\ 0 & N_{I,2}^e & 0\\ 0 & 0 & N_{I,3}^e\\ N_{I,2}^e & 0 & 0\\ 0 & N_{I,3}^e & 0\\ 0 & 0 & N_{I,1}^e\\ N_{I,3}^e & 0 & 0\\ 0 & N_{I,1}^e & 0\\ 0 & 0 & N_{I,2}^e\end{bmatrix}, \tag{A.7}$$

$\mathbf{b}_0$ is the body force, ρ_0 is the mass density at the reference configuration, Ω_0^e is the regular region in $\Re^3$ that is

occupied by the element in the reference configuration, $\bar{\mathbf{s}}$ is the surface traction that may be prescribed as part of the object boundary conditions, $\partial\Omega_0^e \cap \mathcal{S}_{20}$ is part of the boundary of the element where surface traction is prescribed (which may be an empty set), and

$$S = \begin{bmatrix} \sigma_{xx} \\ \sigma_{yy} \\ \sigma_{xz} \\ \sigma_{xy} \\ \sigma_{xz} \\ \sigma_{yz} \end{bmatrix} \tag{A.8}$$

is the stress vector. $\sigma_{\cdot\cdot}$ are the components of the Cauchy stress tensor. The subscript notation is used in (A.7); for example, $\xi_{3,1}$ is the partial derivative of the third component of ξ with respect to its first variable.

In the element equations, the matrix M^e is dense since the element shape functions N_I^e are not typically mutually orthogonal. The matrix M^e is sometimes approximated with a diagonal matrix by using nodal quadrature to decrease computational cost, but this is by no means inherent to the finite element method. The same is true for the function R^e, i.e. the "force" on any node depends on the nodal variables of all the other nodes within the element, as given above in (A.4) and (A.2). Therefore, in FEM formulation, the degrees of freedom are fully connected within an element.

After the element level equations are assembled, the resulting system is in the form

$$M\ddot{\hat{\mathbf{x}}} + R(\hat{\mathbf{x}}) = F, \tag{A.9}$$

which is a system of ordinary differential equations.

For the assembled set of equations, the variables for the elements are connected only by the degrees of freedom shared between elements. This results in a typical banded structure for the matrix M and a similar dependence in the function R.

A.2. Linear elastic material properties

If the displacement gradient is small and the residual stress in reference configuration vanishes, then the stress–strain relationship of the material can be approximated by linearization. Specifically, for an isotropic material, the stress–strain relationship can be parameterized by λ and μ, which are called the Lame's constants.

For three-dimensional elasticity, six components of stress and strain exist and the stresses are related to the strains by Hooke's law as follows:

$$\begin{bmatrix} \sigma_{xx} \\ \sigma_{yy} \\ \sigma_{zz} \\ \sigma_{xy} \\ \sigma_{xz} \\ \sigma_{yz} \end{bmatrix} = \begin{bmatrix} \lambda+2\mu & \lambda & \lambda & 0 & 0 & 0 \\ \lambda & \lambda+2\mu & \lambda & 0 & 0 & 0 \\ \lambda & \lambda & \lambda+2\mu & 0 & 0 & 0 \\ 0 & 0 & 0 & \mu & 0 & 0 \\ 0 & 0 & 0 & 0 & \mu & 0 \\ 0 & 0 & 0 & 0 & 0 & \mu \end{bmatrix} \begin{bmatrix} \varepsilon_{xx} \\ \varepsilon_{yy} \\ \varepsilon_{zz} \\ 2\varepsilon_{xy} \\ 2\varepsilon_{xz} \\ 2\varepsilon_{yz} \end{bmatrix}. \tag{A.10}$$

where $\varepsilon_{\cdot\cdot}$ are the components of the infinitesimal strain tensor.

Two-dimensional elasticity is categorized into two cases: plane strain and plane stress. Plane strain is used when the thickness of an object is large, while plane stress is used when the thickness of an object is small compared to its overall dimensions. Both cases are subset of general three-dimensional elasticity problems. The stress strain relation in plane stress case is given by:

$$\begin{bmatrix} \sigma_{xx} \\ \sigma_{yy} \\ \sigma_{xy} \end{bmatrix} = \begin{bmatrix} \frac{4\mu(\lambda+\mu)}{\lambda+2\mu} & \frac{2\lambda\mu}{\lambda+2\mu} & 0 \\ \frac{2\lambda\mu}{\lambda+2\mu} & \frac{4\mu(\lambda+\mu)}{\lambda+2\mu} & 0 \\ 0 & 0 & \mu \end{bmatrix} \begin{bmatrix} \varepsilon_{xx} \\ \varepsilon_{yy} \\ 2\varepsilon_{xy} \end{bmatrix}, \tag{A.11}$$

and for the plane strain case, it is given by:

$$\begin{bmatrix} \sigma_{xx} \\ \sigma_{yy} \\ \sigma_{xy} \end{bmatrix} = \begin{bmatrix} \lambda+2\mu & \lambda & 0 \\ \lambda & \lambda+2\mu & 0 \\ 0 & 0 & \mu \end{bmatrix} \begin{bmatrix} \varepsilon_{xx} \\ \varepsilon_{yy} \\ 2\varepsilon_{xy} \end{bmatrix}. \tag{A.12}$$

A.3. Lumped element models (LEM)

Lumped element models are meshes of mass, spring and damper elements. Lumped masses at the nodes of the mesh are interconnected by spring and damper elements. The equations of motion are the collection of the Newton's equations written for the individual nodal masses.

For each nodal mass, the equation of motion is in the form

$$m_i\ddot{\mathbf{x}}_i + K_i(\mathbf{x}) = F_i \tag{A.13}$$

with F_i being the external force on the node, such as gravity, and

$$K_i(\mathbf{x}) = \sum_{\{i,j\text{connected}\}} \mathbf{f}(\mathbf{x}_i, \mathbf{x}_j) + \sum_{\{i,j,k\text{connected}\}} \mathbf{g}(\mathbf{x}_i, \mathbf{x}_j, \mathbf{x}_k), \tag{A.14}$$

where $f(\cdot,\cdot)$ is the force from a linear spring and the $g(\cdot,\cdot,\cdot)$ is the force from an angular spring. A typical expression used for linear springs is

$$\mathbf{f}(\mathbf{x}_1, \mathbf{x}_2) = k(\|\mathbf{x}_1 - \mathbf{x}_2\| - L_0)\frac{\mathbf{x}_1 - \mathbf{x}_2}{\|\mathbf{x}_1 - \mathbf{x}_2\|}. \tag{A.15}$$

For the angular springs, the force expression is in the form

$$\mathbf{g}(\mathbf{x}_1, \mathbf{x}_2, \mathbf{x}_3) = k(\theta - \theta_0)\left(\frac{\mathbf{x}_1 - \mathbf{x}_2}{\|\mathbf{x}_1 - \mathbf{x}_2\|} \times \frac{\mathbf{x}_2 - \mathbf{x}_3}{\|\mathbf{x}_2 - \mathbf{x}_3\|}\right) \times \frac{\mathbf{x}_1 - \mathbf{x}_2}{\|\mathbf{x}_1 - \mathbf{x}_2\|}. \tag{A.16}$$

These expressions are for negative force acting on node $\mathbf{x}_1$, due to the a spring between $\mathbf{x}_1$, $\mathbf{x}_2$ and an angular spring between $\mathbf{x}_1$, $\mathbf{x}_2$, $\mathbf{x}_3$. L_0 is the rest length of the linear spring and θ_0 is the rest angle of the angular spring. The angular springs are typically used to enforce $\mathcal{C}^1$ continuity in the mesh. In this work, we use only linear spring for simplicity.

The connectivity in LEM depends on the types of the springs used. The force on any node depends on the nodes that connected to through springs. This results are in a sparse system of equations, similar to the finite element models.

References

[1] Y.C. Fung, Biomechanics: Mechanical Properties of Living Tissues, Springer-Verlag, New York, NY, USA, 1993.

[2] D. Terzopoulos, J. Platt, A. Barr, K. Fleischer, Elastically deformable models, in: SIGGRAPH '87: Proceedings of the 14th Annual Conference on Computer Graphics and Interactive Techniques, ACM, 1987, pp. 205–214.

[3] D.N. Metaxas, Physics-Based Deformable Models: Applications to Computer Vision, Graphics, and Medical Imaging, Kluwer Academic Publishers, Norwell, MA, USA, 1996.

[4] X. Provot, Deformation constraints in a mass-spring model to describe rigid cloth behavior, in: Graphics Interface, 1995, pp. 147–154.

[5] D. Bourguignon, M. Cani, Controlling anisotropy in mass-spring systems, in: Eurographics Workshop on Computer Animation and Simulation (EGCAS), 2000, pp. 113–123.

[6] M. Bro-Nielsen, Finite element modeling in surgery simulation, Proceedings of the IEEE 86 (3) (1998) 490–503.

[7] D.L. James, D.K. Pai, ARTDEFO: accurate real time deformable objects, in: Proceedings of SIGGRAPH 99: 26th International Conference on Computer Graphics and Interactive Techniques, ACM, 1999, pp. 65–72.

[8] S. Cotin, H. Delingette, N. Ayache, Real-time elastic deformations of soft tissues for surgery simulation, IEEE Transactions on Visualization and Computer Graphics 5 (1) (1999) 62–73.

[9] Y. Zhuang, J. Canny, Haptic interaction with global deformations, in: Proceedings of the IEEE International Conference on Robotics and Automation (ICRA 2000), 2000, pp. 2428–2433.

[10] H. Delingette, S. Cotin, N. Ayache, Efficient linear elastic models of soft tissues for real-time surgery simulation, in: J. Westwood et al. (Eds.), Medicine Meets Virtual Reality (MMVR 7), IOS Press, Amsterdam, 1999.

[11] K.D. Costa, P.J. Hunter, J.M. Rogers, J.M. Guccione, L.K. Waldman, A.D. McCulloch, A three-dimensional finite element method for large elastic deformations of ventricular myocardium: part i – cylindrical and spherical polar coordinates, ASME Journal of Biomechanical Engineering 118 (1996) 452–463.

[12] K.D. Costa, P.J. Hunter, J.M. Rogers, J.M. Guccione, L.K. Waldman, A.D. McCulloch, A three-dimensional finite element method for large elastic deformations of ventricular myocardium: part ii – prolate spherical coordinates, ASME Journal of Biomechanical Engineering 118 (1996) 464–472.

[13] X. Wu, M.S. Downes, T. Goktekin, F. Tendick, Adaptive nonlinear finite elements for deformable body simulation using dynamic progressive meshes, in: Proceedings of the EUROGRAPHICS 2001, 2001.

[14] X. Wu, F. Tendick, Multigrid integration for interactive deformable body simulation, in: International Symposium on Medical Simulation (2004), Association for Computing Machinery, Inc., 2004, pp. 92–104.

[15] M. Müller, J. Dorsey, L. McMillan, R. Jagnow, B. Cutler, Stable real-time deformations, in: SCA '02: Proceedings of the 2002 ACM SIGGRAPH/Eurographics Symposium on Computer Animation, 2002, pp. 49–54.

[16] M. Müller, M. Gross, Interactive virtual materials, in: GI '04: Proceedings of Graphics Interface 2004, 2004, pp. 239–246.

[17] M. Nesme, Y. Payan, F. Faure, Efficient, physically plausible finite elements, in: Eurographics (Short Papers), 2005, pp. 77–80.

[18] G. Irving, J. Teran, R. Fedkiw, Invertible finite elements for robust simulation of large deformation, in: SCA '04: Proceedings of the 2004 ACM SIGGRAPH/Eurographics Symposium on Computer animation, 2004, pp. 131–140.

[19] F. Conti, Tissue Modeling via Space Filling Elastic Spheres, Presented at the Stanford Workshop on Surgical Simulation, 2001.

[20] T.W. Sederberg, S.R. Parry, Free-form deformation of solid geometric models, in: Proceedings of SIGGRAPH'86, 1986.

[21] B. Barsky, Computer Graphics and Geometric Modeling Using Beta-Splines, Springer-Verlag, New York, 1988.

[22] A. Joukhadar, F. Garat, C. Laugier, Parameter identification for dynamic simulation, in: Proceedings of the IEEE International Conference on Robotics and Automation (ICRA'97), 1997, pp. 1928–1933.

[23] A. Joukhadar, C. Laugier, Dynamic simulation: Model, basic algorithms, and optimization, in: Algorithms For Robotic Motion and Manipulation, 1997, pp. 419–434.

[24] G. Bianchi, M. Harders, G. Székely, Mesh topology identification for mass-spring models, in: R.E. Ellis, T.M. Peters (Eds.), Medical Image Computing and Computer-Assisted Intervention (MICCAI 2003), vol. 1, Springer, 2003, pp. 50–58.

[25] G. Bianchi, B. Solenthaler, G. Székely, M. Harders, Simultaneous topology and stiffness identification for mass-spring models based on fem reference deformations, in: Medical Image Computing and Computer-Assisted Intervention (MICCAI 2004), vol. 2, 2004, pp. 293–301.

[26] O. Deussen, L. Kobbelt, P. Tucke, Using simulated annealing to obtain good nodal approximations of deformable bodies, in: In Sixth Eurographics Workshop on Simulation and Animation, Springer, 1995, pp. 30–43.

[27] A.V. Gelder, Approximate simulation of elastic membranes by triangulated spring meshes, Journal of Graphics Tools 3 (2) (1998) 21–42.

[28] A. Maciel, R. Boulic, D. Thalmann, Deformable tissue parameterized by properties of real biological tissue, in: IS4TH, Springer, 2003, pp. 74–87.

[29] V. Baudet, M. Beuve, F. Jaillet, B. Shariat, F. Zara, New Mass-Spring System Integrating Elasticity Parameters in 2d, Tech. Rep. RR-LIRIS-2007-003, LIRIS, UniversitT Lyon 1 (February 2007).

[30] V. Baudet, M. Beuve, F. Jaillet, B. Shariat, F. Zara, Integrating Tensile Parameters in 3d Mass-Spring System, Tech. Rep. RR-LIRIS-2007-004, LIRIS, UniversitT Lyon 1 (February 2007).

[31] M.C. Çavuşoğlu, Telesurgery and Surgical Simulation: Design, Modeling, and Evaluation of Haptic Interfaces to Real and Virtual Surgical Environments, Ph.D. Thesis, EECS Department, University of California, Berkeley, 2000.

[32] B.A. Lloyd, G. Székely, M. Harders, Identification of spring parameters for deformable object simulation, IEEE Transactions on Visualization and Computer Graphics 13 (2007) 1081–1094.

[33] X. Wang, V. Devarajan, 1D and 2D structured mass-spring models with preload, The Visual Computer 21 (7) (2005) 429–448.

[34] X. Wang, V. Devarajan, Improved 2D mass-spring-damper model with unstructured triangular meshes, The Visual Computer 24 (1) (2007) 57–75.

[35] H. Delingette, Triangular springs for modeling nonlinear membranes, IEEE Transactions on Visualization and Computer Graphics 14 (2) (2008) 329–341.

[36] H. Delingette, Biquadratic and quadratic springs for modeling St. Venant Kirchhoff materials, in: ISBMS '08: Proceedings of the 4th International Symposium on Biomedical Simulation, 2008, pp. 40–48.

[37] D. d'Aulignac, C. Laugier, M.C. Çavuşoğlu, Towards a realistic echographic simulator with force feedback, in: Proceedings of the IEEE/RSJ International Conference on Intelligent Robotics and Systems (IROS 1999), 1999, pp. 727–732.

[38] M.C. Çavuşoğlu, T. Goktekin, F. Tendick, GiPSi: a framework for open source/open architecture software development for organ level surgical simulation, IEEE Transactions on Information Technology in Biomedicine 10 (2) (2006) 312–321.

[39] T. Klemens, E. Lund, B.F. Srensen, Optimal shape of thin tensile test specimen, Journal of the American Ceramic Society 90 (2007) 1827–1835.

[40] J.N. Reddy, An Introduction to the Finite Element Method, second ed., McGraw-Hill, Inc., 1993.

[41] K. Bathe, Finite Element Procedures, Prentice-Hall, Inc., Englewood Cliffs, NJ, USA, 1996.

[42] M.E. Gurtin, An Introduction to Continuum Mechanics, Academic Press, New York, NY, USA, 1981.

[43] M.E. Gurtin, Topics in Finite Elasticity, Society for Industrial and Applied Mechanics, Philadelphia, PA, USA, 1981.

[44] J.E. Marsden, T.J.R. Hughes, Mathematical Foundations of Elasticity, Prentice-Hall, Inc., Englewood Cliffs, NJ, USA, 1983.